The Relation between Soil Water Repellency and Water Content Can Be Predicted by Vis-NIR Spectroscopy

Hermansen, Cecilie; Moldrup, Per; Müller, Karin; Knadel, Maria; de Jonge, Lis Wollesen

Published in:
Soil Science Society of America Journal

DOI (link to publication from Publisher):
10.2136/sssaj2019.03.0092

Publication date:
2019

Document Version
Publisher's PDF, also known as Version of record

The Relation between Soil Water Repellency and Water Content Can Be Predicted by Vis-NIR Spectroscopy

Cecilie Hermansen*
Dep. of Agroecology
Faculty of Science and Technology
Aarhus Univ.
Blichers Allé 20, PO Box 50
DK-8830 Tjele, Denmark

Per Moldrup
Dep. of Civil Engineering
Aalborg Univ.
Thomas Manns Vej 23
DK-9200 Aalborg East, Denmark

Karin Müller
New Zealand Institute for Plant & Food Research Limited (PFR)
Land Use Impacts
Hamilton, New Zealand

Maria Knadel
Lis Wollesen de Jonge
Dep. of Agroecology
Faculty of Science and Technology
Aarhus Univ.
Blichers Allé 20, PO Box 50
DK-8830 Tjele, Denmark

The severity of soil water repellency (SWR) varies nonlinearly with water content (w), and it is extremely laborious to obtain complete SWR-w curves, which are needed to predict the occurrence of SWR. In this study, we combined a three-parameter moisture-dependent SWR (MD-SWR) model with visible near-infrared spectroscopy (vis-NIRS) as a fast and novel method to estimate the SWR-w curve. The method was applied to a data set of SWR-w curves determined for 71 soil samples (organic carbon [OC] content: 0.021–0.147 kg kg^{-1}, clay: 0.000–0.520 kg kg^{-1}). The degree of SWR was measured on air-dried soil samples (SWR_{AD}) and on soil samples with increasing water contents until the water content at which the soils became wettable (w_{NON}) was reached. The three-parameter MD-SWR model was fitted to the measured SWR-w curves between the water content at air-dry conditions (w_{AD}) and w_{NON}. The total SWR was then calculated as the trapezoidal integrated area underneath the SWR-w curves (SWR_{AREA}). Air-dried soil samples were scanned with a vis-NIR spectrometer. Each of the three MD-SWR model parameters was correlated to vis-NIRS spectra using partial least squares regression. The SWR_{AREA} was predicted using two approaches. For Approach I, the SWR_{AREA} calculated from the MD-SWR model was predicted with a single vis-NIRS model. Approach II utilized predicted MD-SWR model parameter values to obtain vis-NIRS-predicted SWR-w curves between w_{AD} and w_{NON}, and the SWR_{AREA} was calculated from these curves. Results show that vis-NIRS can predict the shape of the SWR-w curves as well as the SWR_{AREA} (R^2 = 0.58 and 0.56 for Approach I and II, respectively) across a highly variable dataset from a single vis-NIRS scanning and one SWR measurement at air-dried conditions.

Abbreviations: iPLSR, interval partial least squares regression; OC, organic carbon; PLSR, partial least squares regression; PSD, particle-size distribution; RMSEC, root mean square error of calibration; RMSECV, root mean square error of cross-validation; RPIQ, ratio of performance to interquartile range; SNV, standard normal variate; SWR, soil water repellency; vis-NIRS, visible near-infrared spectroscopy.

Core Ideas

- **Soil water repellency (SWR) and water content (w) curves were compared for 71 soil samples.**
- **SWR-w relations were highly variable across the soil samples from New Zealand.**
- **A three-parameter SWR-w model described well the measured SWR-w data.**
- **Vis-NIRS could successfully predict all three SWR-w model parameters.**
- **Two methods for predicting total area under the SWR-w curve by vis-NIRS are presented.**

Soil water repellency (SWR) is a soil property that degrades soil functions (de Jonge et al., 2009) and reduces agricultural production (Franco et al., 1995; Müller et al., 2010). The degradation of soil functions includes reduced infiltration (Leighton-Boyce et al., 2007; Müller et al., 2010), altered filtering capacity of pesticides and nutrients (Dekker and Ritsema, 1995; de Jonge et al., 2009; Müller et al., 2010; Müller et al., 2014), increased overland flow and erosion (Osborn et al., 1964; Leighton-Boyce et al., 2007), and increased finger flow (Dekker and Ritsema, 1995; de Jonge et al., 2009).

Soils in New Zealand have a high propensity to develop water-repellent conditions. Two surveys under pastoral land use across the North Island and South Island found that 98% (Deurer et al., 2011) and 92% (Hermansen et al., 2019) of the collected soil samples exhibited the potential to develop water repellency.

Soil Sci. Soc. Am. J. 83:1616–1627
doi:10.2136/sssaj2019.03.0092
Received 30 Mar. 2019.
Accepted 14 Aug. 2019.
*Corresponding author (cecilie.hermansen@agro.au.dk).

However, soils are not always water-repellent, and the severity of SWR varies as a nonlinear function of soil-water content (w). Soils can become hydrophobic within a confined range of w, delimited by an upper critical w (w_{NON}), above which the soil again becomes hydrophilic (de Jonge et al., 2007; Kawamoto et al., 2007; Regalado et al., 2008). Soil organic matter covering mineral particles and aggregates can reorient and expose either hydrophilic or hydrophobic ends depending on the w, which changes the surface tension of the soil and causes shifts between hydrophobic and hydrophilic conditions (de Jonge et al., 1999; Doerr et al., 2000; Roy and McGill, 2000; Graber et al., 2009). Soil organic matter content might be the one soil property that has the greatest impact on the SWR of New Zealand pastoral soil, and a linear relation between w_{NON} and organic carbon (OC) has been suggested as a guide for irrigation practices and to prevent the occurrence of SWR and associated degradation of soil functions (Hermansen et al., 2019).

The severity of SWR can be described by a SWR characteristic curve, with SWR as a function of gravimetric (de Jonge et al., 2007; Regalado et al., 2008; Regalado and Ritter, 2009b) or volumetric w (Regalado and Ritter, 2009a; Karunarathna et al., 2010a), or in terms of pF values (de Jonge et al., 2007; Karunarathna et al., 2010b). The area underneath the SWR-w curve represents the total SWR of a soil (SWR_{AREA}). The molarity of an ethanol droplet (MED) test assesses the degree of SWR as the liquid surface tension of an ethanol droplet, which infiltrates into a soil in 5 s (King, 1981; de Jonge et al., 1999; Kawamoto et al., 2007). The SWR-w curve may start from 0 kg kg^{-1} w in the oven-dry (de Jonge et al., 1999; de Jonge et al., 2007) or air-dry state (w_{AD}) (Karunarathna et al., 2010a; Karunarathna et al., 2010b) and continue until the soil becomes hydrophilic at w_{NON}. The dry end of the SWR-w curve obtained from oven-drying can indicate whether the severity of SWR might be affected by heating depending on the OC quality (de Jonge et al., 1999).

The shape of the curve for hydrophobic soils is nonlinear, and the SWR-w curve is either unimodal or bimodal (de Jonge et al., 1999; Regalado et al., 2008). Bimodal SWR-w curves are hydrophobic at oven-dry conditions, but with increasing w the severity of SWR decreases to a local minimum at which the soil maintains some hydrophobicity or becomes temporarily hydrophilic (de Jonge et al., 1999; de Jonge et al., 2007). After the first peak, the severity of SWR increases once more until it reaches a local maximum after which it decreases toward w_{NON}. The global maximum might be located in either of the two peaks (Regalado et al., 2008), but most soils exhibit the highest severity within the second peak, thus associated with the higher w. Soils with a unimodal SWR-w curve are either hydrophobic in oven-dry conditions or hydrophilic, after which they become hydrophobic as w increases before or after w_{AD}.

The conventional laboratory method for obtaining SWR-w curves is extremely time-consuming, but might nevertheless contain implicit errors in w_{NON} and the estimation of SWR_{AREA} because the severity of SWR is measured in discrete w steps (Regalado et al., 2008). Different mathematical models have been proposed to provide a continuous fit to the SWR-w curve (Bachmann et al., 2007; Regalado and Ritter, 2009b; Regalado and Ritter, 2009a; Karunarathna et al., 2010a; Karunarathna et al., 2010b). Karunarathna et al. (2010a) developed a model for predicting the SWR-w curves for 19 Japanese and Danish soil samples with OC contents ranging from 0.011 to 0.141 kg kg^{-1}. This model has three fitting parameters, including the maximum degree of SWR (SWR_{MAX}), the w at SWR_{MAX} (w_{MAX}), and the w_{NON}. Within that study, all three fitting parameters could be described by the OC content through a logarithmic function. Some other studies have found that w_{MAX}, and w_{NON} can be described by a linear correlation to OC content (de Jonge et al., 2007; Kawamoto et al., 2007; Regalado et al., 2008). The Karunarathna et al. (2010a) model has furthermore two fixed parameters, including the SWR at air-dried conditions (SWR_{AD}) and the corresponding w (w_{AD}), which are both directly related to the shape of the SWR-w curve. Another study suggested a two-region model to describe the SWR-w curve shape on Japanese soil samples with OC contents between 0.006 and 0.141 kg kg^{-1} and clay contents between 0.130 and 0.233 kg kg^{-1} (Karunarathna et al., 2010b). By plotting the severity of SWR as a function of soil matric potential, they observed a linear increase in SWR between w_{AD} and w_{MAX} (defined as region 1) following a linear decrease in SWR from w_{MAX} to w_{NON} (defined as region 2). Thus, for each region they correlated the slope and intercept of the SWR-w curve to OC content, making it possible to obtain the SWR-w curve by estimating these four parameters.

Visible near-infrared spectroscopy (vis-NIRS) is a fast method used to predict a wide range of basic and functional soil properties (Stenberg et al., 2010; Katuwal et al., 2018; Knadel et al., 2018). Throughout the visible range (400–700 nm) the spectrum is affected by overlapping absorptions from iron oxides and organic matter, whereas the near-infrared range (700–2500 nm) is dominated by overtones and combinations of OH, CH, CO, NH, and Al-OH originating from fundamental vibrations in the mid-infrared range (Hunt, 1977; Clark, 1999; Chang et al., 2001). Thus, vis-NIRS spectra contain direct spectral responses from soil moisture, clay and OC contents and quality. It is well documented that vis-NIRS can predict the OC content of soils (Chang et al., 2001; Stenberg et al., 2010; Knadel et al., 2012; Peng et al., 2014; Hermansen et al., 2016). However, soil properties that do not give a direct spectral response have also been successfully predicted using vis-NIRS. For example, Kim et al. (2014) predicted the degree of SWR and water drop penetration time on New Zealand soil samples from the North Island dried at 65°C. Further, Knadel et al. (2016) predicted the degree of SWR for Danish soil samples collected across a homogeneous agricultural field at air-dry conditions and after drying at 60 and 105°C, respectively. However, it would be advantageous, if the entire SWR-w curve could be obtained from vis-NIRS spectra. Hermansen et al. (2017) predicted the continuous particle-size distribution (PSD) curve by fitting two PSD functions to measured data after which the fitting parameters of each PSD function were predicted with vis-NIRS for 431 Danish soil samples covering USDA textural classes between

sand and silty clay. The two PSD functions had two and three fitting parameters, respectively, and both functions performed well in combination with vis-NIRS. A similar approach has been applied in other studies to predict the soil-water retention curve (Babaeian et al., 2015; Pittaki-Chrysodonta et al., 2018). However, no studies have yet examined the possibility of adopting this approach to obtain the SWR-*w* curve function.

Since the vis-NIRS spectral range contains responses from various soil components, a variable selection method can be applied to leave out less relevant variables from the spectrum. This can reduce model complexity (Zou et al., 2010) and indicate which spectral regions are most important for predicting the different soil properties. The variable selection method of interval partial least squares regression (iPLSR) has previously been applied successfully for the selection of important spectral regions for some soil parameters related to the PSD curve (Hermansen et al., 2017) and soil specific surface area (Knadel et al., 2018).

For this study, we examined the ability of vis-NIRS to predict the three fitting parameters of the Karunarathna et al. (2010a) function (SWR_{MAX}, w_{MAX}, and w_{NON}) to yield a vis-NIRS prediction of the continuous SWR-*w* curve between w_{AD} and w_{NON}. We chose the Karunarathna et al. (2010a) function, since the number of fitting parameters for vis-NIRS prediction should be limited to avoid error propagation (Hermansen et al., 2017). Also, a successful vis-NIRS prediction requires a direct or indirect response in the spectrum, and each fitting parameter in this function has previously been related to spectrally active OC.

Thus, the objectives were to obtain the SWR-*w* curve from one SWR measurement and one vis-NIRS scanning at air-dry conditions, by (i) fitting the Karunarathna et al. (2010a) function to SWR-*w* curves for New Zealand soil samples between w_{AD} and w_{NON}, (ii) utilizing the variable selection method of interval partial least squares (iPLSR) to find important spectral regions for the severity of SWR throughout the vis-NIRS spectral range, (iii) predicting the three fitting parameters (SWR_{MAX}, w_{MAX}, and w_{NON}) of the Karunarathna et al. (2010a) function with vis-NIRS, (iv) applying the vis-NIRS-predicted fitting parameters and measured SWR at air-dried conditions to yield SWR-*w* curves, and (v) predicting the SWR_{AREA} with vis-NIRS.

MATERIALS AND METHODS

Sites and Soil Sampling

Between 5 and 17 Jan. 2012, 78 soil samples were collected from 26 permanent pastures, which were spread across the dominant soil orders under pasture in New Zealand's South Island: Brown (B), Pallic (P), Podzol (Z) and Recent (R) soils (Hewitt, 2010) plus the soil order Semiarid (S), which is prevalent in the Otago region (Fig. 1). These soil orders, classified according to New Zealand's soil classification system, correspond to Cambisols, Luvisols, Podzols, Fluvisols and Arenosols in the classification of the World Reference Base for Soil Resources (IUSS Working Group WRB, 2006), respectively. Site selection was stratified within each of the soil orders using three vectorized summer rainfall classes: L ≤ 150 mm (low), M = 150 to 350 mm (medium), and H ≥ 350 mm (high) based on rainfall data for the 30-yr period 1971 to 2000, assuming that summer rainfall influences the occurrence of SWR. Details of the site selection can be found in Hermansen et al. (2019). At each site, three bulk soil samples from the top 0- to 5-cm mineral soil were taken along a transect with samples approximately 10 m apart. The soil was sieved to <2 mm, air-dried, and subsamples were analyzed for texture on a Malvern laser sizer and OC content using a Leco Truspec instrument (Blakemore et al., 1987).

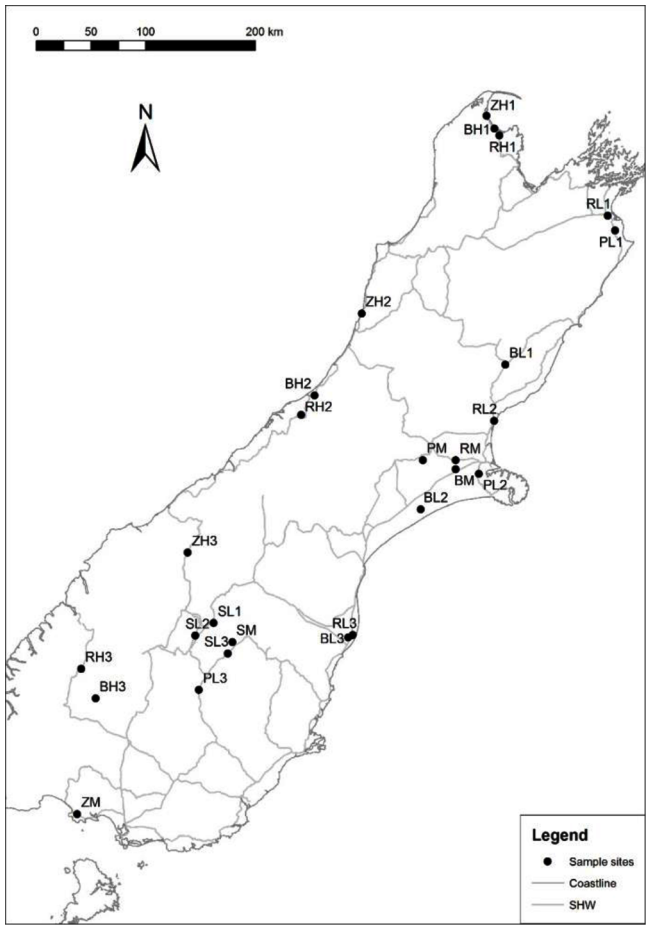

Fig. 1. Twenty-six sampling sites across the South Island of New Zealand. The sampling sites represent five soil orders: Brown (B), Pallic (P), Podzol (Z), Recent (R), and Semiarid (S) and were partitioned into three summer rainfall classes: L ≤ 150 mm (low), M = 150 to 350 mm (medium), H ≥ 350 mm (high). SHW, state highway networks.

Six samples of the 78 samples were hydrophilic (three Semiarid soil samples and three Recent soil samples from two locations) (Hermansen et al., 2019). Further, one Podzol soil sample was extreme in OC content at 0.217 kg kg^{-1} and was regarded as an outlier as it would otherwise highly influence vis-NIRS predictions. Thus, 71 samples from 24 locations were used in this study.

Soil Water Repellency Measurements

Prior to SWR measurements, tap water was pipetted onto air-dried soil samples to reach specific soil water contents in the *w* interval from w_{AD} to w_{NON}. After addition of water, the soil was gently mixed and left in sealed plastic bags for at least 2 wk to equilibrate in the dark in a temperature controlled laboratory (20°C). The

SWR was measured following the protocol for the MED test (de Jonge et al., 1999; Roy and McGill, 2002; Kawamoto et al., 2007; Hermansen et al., 2019). We prepared ethanol and deionized water solutions, with the concentration of ethanol ranging from 0.01 to 0.80 $m^3\ m^{-3}$ in steps of 0.01 $m^3\ m^{-3}$. We pipetted 60 μL of ethanol solution onto a plain soil surface, and the degree of SWR was determined as the highest ethanol concentration that did not infiltrate within 5 s, after which this concentration was translated to the liquid surface tension of ethanol (γ) following the equation of Roy and McGill (2002): $\gamma = 61.05 - 14.75 \ln(M + 0.5)$, where M is the molarity of ethanol. After each SWR measurement, we determined gravimetric w by oven-drying the samples at 105°C.

Fitting the Karunarathna Function

The Karunarathna et al. (2010a) function is a curvilinear, simplified β function, which gives a unimodal shape of the SWR-w curve between w_{AD} and w_{NON}. This function was originally developed to represent the contact angle as a function of volumetric w. We modified the function to represent surface tension as a function of gravimetric w. We accounted for the fact that the aqueous concentration of ethanol increases as the liquid surface tension decreases, by calculating SWR input values as the difference of "71.27 – SWR", with 71.27 mN m^{-1} being the surface tension of water. As a result, relatively low and high severities of SWR were characterized by relatively low and high numerical values.

The function was fitted onto each SWR-w curve between w_{AD} and w_{NON} for 71 soil samples using the Microsoft Excel Solver function (Generalized Reduced Gradient). The function has five input parameters:

$$71.27-\mathrm{SWR}(w)=(71.27-\mathrm{SWR}_{AD}) + \left\{\left[(71.27-\mathrm{SWR}_{MAX})-(71.27-\mathrm{SWR}_{AD})\right] \times\left(\frac{w_{NON}-w}{w_{NON}-w_{MAX}}\right)\left(\frac{w-w_{AD}}{w_{MAX}-w_{AD}}\right)^{\frac{w_{MAX}-w_{AD}}{w_{NON}-w_{MAX}}}\right\} \quad [1]$$

The SWR_{AD} is the degree of SWR at air-dried conditions, and the w_{AD} is the water content at SWR_{AD}. These two input parameters are assumed to be measured (Fig. 2). The three fitting parameters are SWR_{MAX}, which is the maximum level of SWR; w_{MAX}, the water content at SWR_{MAX}; and w_{NON}, the critical water content (Fig. 2). A good correlation between the fitted and measured values for these three parameters has previously been shown (R^2 between 0.90 and 0.99) (Karunarathna et al., 2010a). If $w \geq w_{NON}$, the degree of SWR, expressed as 71.27 – SWR, was 0 mN m^{-1}. It should be noted that for many soil samples, there was a local decrease in the degree of SWR just after air-dried conditions, which might have affected the fit of the function. The reference SWR_{AREA} was obtained as the integrated trapezoidal area underneath the fit of Eq. [1] (Fig. 2).

Visible Near-Infrared Spectroscopy Measurements

We used a bench-top vis-NIRS spectrometer (DS2500, FOSS, Denmark) to measure the diffuse reflectance (R) between 400 and 2500 nm, with a spectral sampling interval of 0.5 nm. Using a white FOSS check sample (FOSS Denmark), the stability of the instrument was checked prior to spectral measurements of the soil samples. The soil samples (air-dried and 2-mm sieved) were placed in a sample cup with a quartz window. The spectrometer automatically rotated the cup while measuring to obtain scans at seven positions on the sample surface, which were subsequently averaged to one spectrum and converted to absorbance (A); $A = \log(1/R)$.

Multivariate Data Analysis

The multivariate analyses were performed in PLS Toolbox version 8.6.2 (Eigenvector Research Inc.), and multivariate calibration models were established with partial least squares regression (PLSR) using the SIMPLS algorithm (de Jong, 1993). The SWR_{AREA} was vis-NIRS-predicted following two approaches. For Approach I, the SWR_{AREA} was calculated from Eq. [1] and vis-NIRS-predicted with PLSR using vis-NIRS spectra, with the SWR_{AREA} being the dependent y-variable. For Approach II, the three fitting parameters of Eq. [1] (71.27 – SWR_{MAX}, w_{MAX}, and w_{NON}) were predicted using three vis-NIRS models and then used as

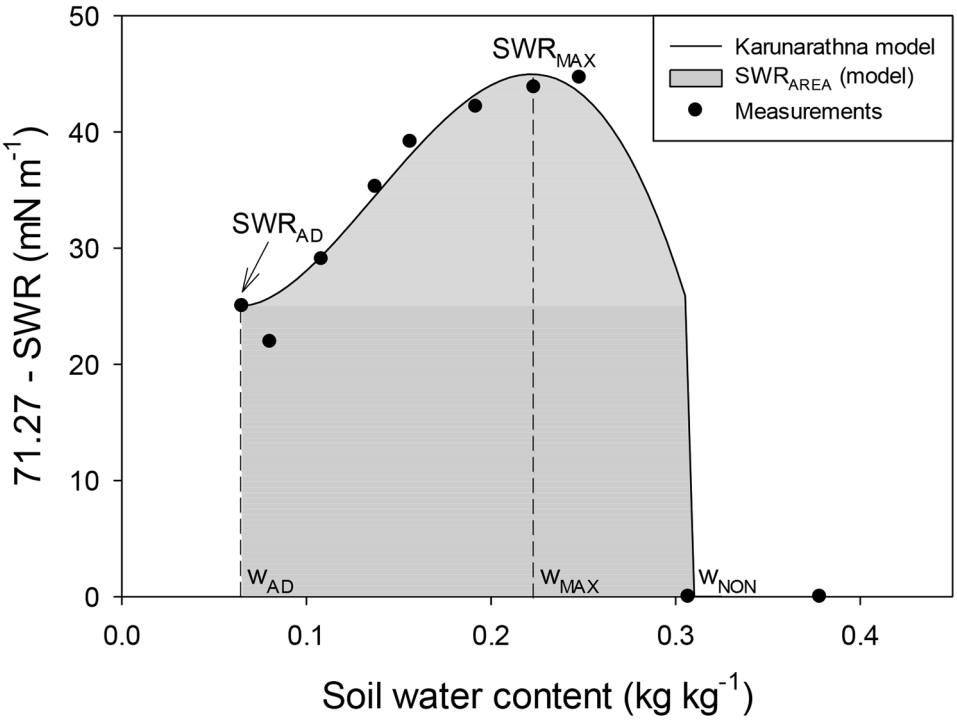

Fig. 2. Soil water repellency versus water content. The Karunarathna et al. (2010a) model has five input parameters, which include measurements of the SWR at air-dried conditions (SWR_{AD}) and the water content at SWR_{AD} (w_{AD}). The model includes three fitting parameters which are the maximum level of SWR (71.27 – SWR_{MAX}), the water content at 71.27 – SWR_{MAX} (w_{MAX}) and the critical soil water content (w_{NON}).

inputs to Eq. [1] to obtain vis-NIRS-predicted SWR-*w* curves, from which we obtained the SWR_{AREA}.

Thus, a vis-NIRS PLSR model was established for each of the three fitting parameters of Eq. [1] (71.27 – SWR_{MAX}, w_{MAX}, and w_{NON}), SWR_{AREA} (Approach I) and OC. An identical procedure for establishing the PLSR models was followed for all parameters to be predicted. First, different spectral standard pretreatment methods were tested to optimize the correlation between spectra and each of the five parameters. The tested pretreatments were detrending (third polynomial), standard normal variate (SNV) (Barnes et al., 1989) and Savitzky-Golay first and second derivatives (Savitzky and Golay, 1964). Then we applied the variable selection method forward iPLSR on pretreated spectra, to remove less important spectral information. The iPLSR method is an automated function in PLS Toolbox 8.6.2, which while running forward divides the spectrum into *n* equally sized intervals and then builds PLSR models on each consecutive spectral interval. The spectral interval that obtains the lowest prediction error is retained. This interval is then tested together with the remaining intervals, and the two intervals that in combination result in the lowest prediction error are retained. This loop is continued until the prediction error no longer decreases, although more intervals are included (Nørgaard et al., 2000; Zou et al., 2010). Since iPLSR is sensitive to the spectral interval sizes (Andersen and Bro, 2010), we tested interval sizes between 40 and 80 nm for each of the five soil parameters. The spectral intervals found by iPLSR were subsequently applied to predict each soil parameter with PLSR and ten-fold cross-validation. For cross-validation, the soil samples were grouped according to soil order, and every 10th sample was systematically included in the same cross-validation set.

The vis-NIRS-predicted values of 71 soil samples for the three fitting parameters of Eq. [1] and laboratory-measured values of SWR_{AD} and w_{AD} were used as input values to obtain the vis-NIRS-predicted SWR-*w* curves. If the vis-NIRS-prediction of w_{MAX} was less than w_{AD} or above w_{NON}, the vis-NIRS-prediction of that specific SWR-*w* curve was classified as unsuccessful. This resulted in four predictions being classified as unsuccessful (one Pallic soil sample, two Recent soil samples and one Semiarid soil sample). These unsuccessful visN-IRS-predictions were excluded prior to the SWR_{AREA} predictions, and we therefore used 67 soil samples to obtain the SWR_{AREA} in Approach I and II.

The model accuracy was evaluated in terms of the root mean square error of calibration (RMSEC) and cross-validation (RMSECV), coefficient of determination (R^2), and ratio of performance to interquartile range (RPIQ).

The RPIQ can be applied as a model accuracy index for datasets that do not follow a normal distribution (Bellon-Maurel et al., 2010), which was appropriate for this dataset, since all soil properties except the SWR_{AREA} and w_{NON} were not normally distributed. The RPIQ is calculated as $RPIQ = (Q_3 - Q_1)/RMSE$, where Q_1 and Q_3 are the first and third quartiles of the dataset. A relatively higher RPIQ value indicates a better model performance.

Table 1. Statistics for 71 New Zealand soil samples representing five soil orders (Brown, Pallic, Podzol, Recent, and Semiarid). Organic carbon; three fitting parameters for the Karunarathna et al. (2010a) model: maximum level of SWR (71.27 – SWR_{MAX}), water content at SWR_{MAX} (w_{MAX}), critical soil water content (w_{NON}). The trapezoidal integrated area (SWR_{AREA}) underneath the SWR-*w* curve was obtained from the continuous Karunarathna et al. (2010a) model fit.

Statistic	Brown *n* = 21	Pallic *n* = 12	Podzol *n* = 11	Recent *n* = 18	Semiarid *n* = 9	All *n* = 71
			Organic carbon			
			kg kg^{-1}			
Min.	0.037	0.024	0.048	0.021	0.025	0.021
Max.	0.096	0.055	0.147	0.068	0.061	0.147
S.d.	0.019	0.007	0.029	0.012	0.013	0.024
Median	0.061	0.037	0.074	0.041	0.039	0.047
Q_1 †	0.045	0.035	0.069	0.035	0.031	0.038
Q_3 ‡	0.078	0.039	0.096	0.048	0.045	0.066
			71.26 – SWR_{MAX}			
			mN m^{-1}			
Min.	35.66	27.69	34.78	18.00	12.00	12.00
Max.	46.72	41.51	45.48	46.31	44.29	46.72
S.d.	3.10	4.38	3.67	7.28	10.94	6.90
Median	40.64	35.02	41.53	42.43	30.07	39.58
Q_1	39.08	32.19	38.34	37.59	26.39	36.08
Q_3	42.43	38.87	43.27	45.03	39.04	42.81
			w_{MAX}			
			kg kg^{-1}			
Min.	0.042	0.051	0.148	0.022	0.082	0.022
Max.	0.320	0.118	0.222	0.179	0.214	0.320
S.d.	0.076	0.020	0.019	0.051	0.041	0.061
Median	0.139	0.092	0.195	0.119	0.096	0.120
Q_1	0.092	0.085	0.186	0.064	0.090	0.090
Q_3	0.206	0.097	0.205	0.157	0.127	0.178
			w_{NON}			
			kg kg^{-1}			
Min.	0.119	0.071	0.220	0.050	0.094	0.050
Max.	0.438	0.206	0.309	0.263	0.293	0.438
S.d.	0.092	0.049	0.027	0.068	0.064	0.082
Median	0.224	0.140	0.274	0.173	0.136	0.195
Q_1	0.165	0.109	0.267	0.148	0.100	0.140
Q_3	0.287	0.184	0.284	0.240	0.178	0.261
			SWR_{AREA}			
			mN m^{-1} kg kg^{-1}			
Min.	3.37	0.79	6.22	1.14	0.12	0.12
Max.	11.57	6.32	8.85	8.32	8.84	11.57
S.d.	2.21	1.92	0.94	2.24	2.81	2.54
Median	5.51	2.75	6.84	4.58	1.74	5.31
Q_1	3.87	1.34	6.56	3.01	0.62	3.20
Q_3	7.22	4.12	7.67	6.67	4.24	6.73

† Q_1, first quartile of the data set.
‡ Q_3, third quartile of the data set.

RESULTS AND DISCUSSION

Soil Properties

The soil samples represented five soil orders collected across the South Island of New Zealand (Fig. 1). The OC content ranged from 0.021 to 0.147 kg kg^{-1}, and the Podzols were highest in OC content (Table 1). The clay content ranged from 0 to 0.52 kg kg^{-1},

and the soil samples covered eight textural classes from sand to silty clay across the USDA textural triangle (Fig. 3). The Brown soils had the widest distribution in texture, and represented seven of the eight classes. In comparison, the Podzols had a narrow distribution and represented only the silty loam and silty clay loam classes.

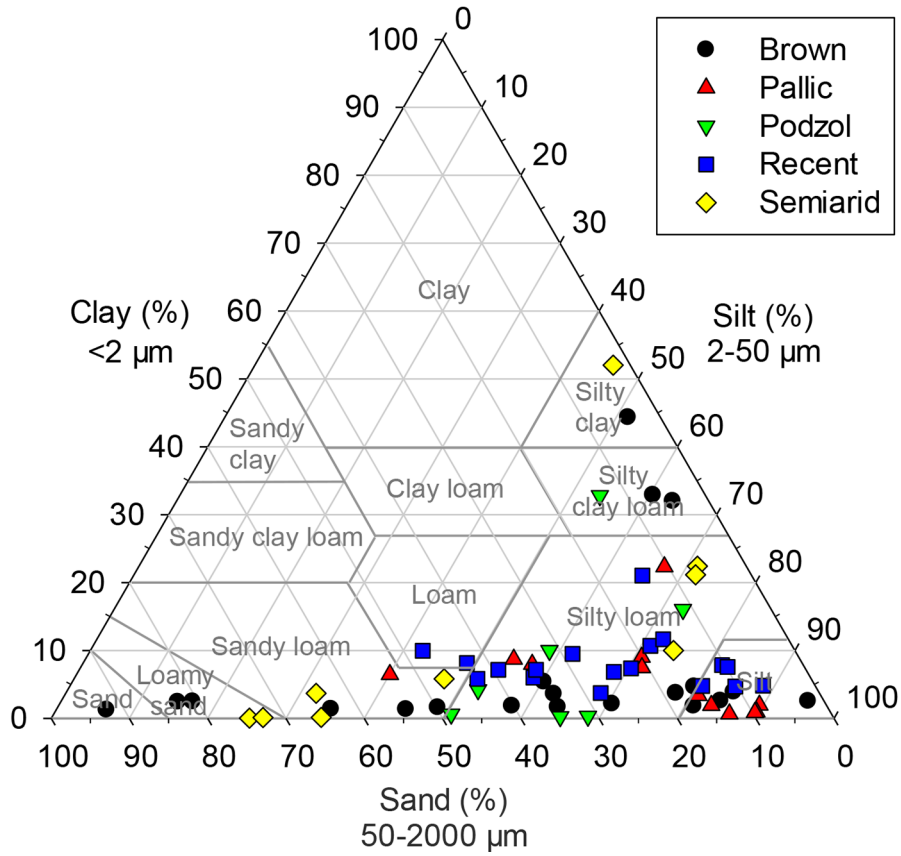

Fig. 3. USDA soil texture triangle of 71 water-repellent soil samples from the South Island of New Zealand. The soil samples were sampled across five soil orders (Brown, Pallic, Podzol, Recent, and Semiarid).

Soil Water Repellency vs. Water Content Curves

The measured SWR-*w* curves exhibited a wide or narrow variation in curve shape and extent depending on the soil order. The Brown soils exhibited the largest range in SWR_{AREA} (3.37–11.57 mN m^{-1} kg kg^{-1}) and w_{NON} (0.119–0.438 kg kg^{-1}) (Table 1), and apparently the highest variability in SWR-*w* curve shapes (Fig. 4a). Conversely, the Podzols represented the narrowest range in SWR_{AREA} (6.22–8.85 mN m^{-1} kg kg^{-1}) and w_{NON} (0.220–0.309 kg kg^{-1}) and the least apparent dispersion in SWR-*w* curve shapes (Fig. 4c). This reflects the fact that the Brown soils covered the widest range in soil textural classes and that the Podzols covered the smallest textural range. The Pallic, Recent and Semiarid soils also exhibited a large variation in curve shapes. Each individual SWR-*w* curve is illustrated in Hermansen et al. (2019).

Altogether, this dataset represented a wide variation in SWR-*w* curves, with 71.27 − SWR_{MAX} ranging from 12.00 to 46.72 mN m^{-1}, w_{MAX} from 0.022 to 0.320 kg kg^{-1}, w_{NON} from 0.050 to 0.438 kg kg^{-1}, and the SWR_{AREA} obtained from Eq. [1] ranging from 0.12 to 11.57 mN m^{-1} kg kg^{-1}. The Karunarathna et al. (2010a) function described the variation in SWR-*w* curve shapes well (Fig. 4), since there was a good correlation between SWR_{AREA} calculated from the measured and fitted curves (R^2 = 0.98) (results not shown). The measured SWR-*w* curves were either hydrophobic or hydrophilic at air-dried conditions. However, some soil samples exhibited lower SWR just after air-dried conditions, which reduced the accuracy of the model fit for some soils, although the fit still followed the overall curve shape (e.g., Fig. 4a and 4e). Further, Eq. [1] did not fit well to the soil sample with the smallest SWR_{AREA} within the Recent soil order (Fig. 4d), which could be caused by a narrow range in *w* at which the soil was hydrophobic combined with a decrease in SWR just after air-dried conditions.

The SWR_{AREA} obtained from Eq. [1] correlated with OC with an R^2 value of 0.46 and RMSE of 1.83 mN m^{-1} kg kg^{-1} (Fig. 4f). The linear regression was performed with 67 samples, for which we had successful vis-NIRS predictions of SWR-*w* curves. Previous studies found that OC or soil organic matter content can describe 60% to 82% of the variation in SWR_{AREA} (de Jonge et al., 1999; Regalado and Ritter, 2005; Regalado et al., 2008; Hermansen et al., 2019). Knowing that SWR depends on both OC content and quality (de Jonge et al., 1999), the lower correlation between SWR_{AREA} and OC than in the literature might be caused by varying quality of OC in this data set representing five soil orders. Although all soils were collected under pasture for this study, we did not attempt to differentiate between pasture types or stock classes. Further, the samples represented areas of varying summer rainfall and soil development. For example, the Brown, Pallic, Podzol, and Semiarid soils are mature soils, whereas the Recent soils are young soils (Hewitt, 2010; Hewitt, 2013). All these factors could potentially have affected the quality of organic matter.

Qualitative Analysis of Vis-NIR Spectra

We found that detrending followed by SNV performed best for all PLSR models. In combination, detrending and SNV reduced multivariate effects, baseline shifts and nonlinearity from the spectra. For the qualitative analysis of vis-NIRS spectra, the pretreated spectra were averaged within each soil order (Fig. 5). Within the visible range, the spectra exhibited a peak in absorbance between 487 and 502 nm. These peaks are located in a spectral range with absorbance originating from different iron oxide species such as hematite and goethite (Scheinost et al., 1998). Further, the Podzols had a plateau in absorbance between

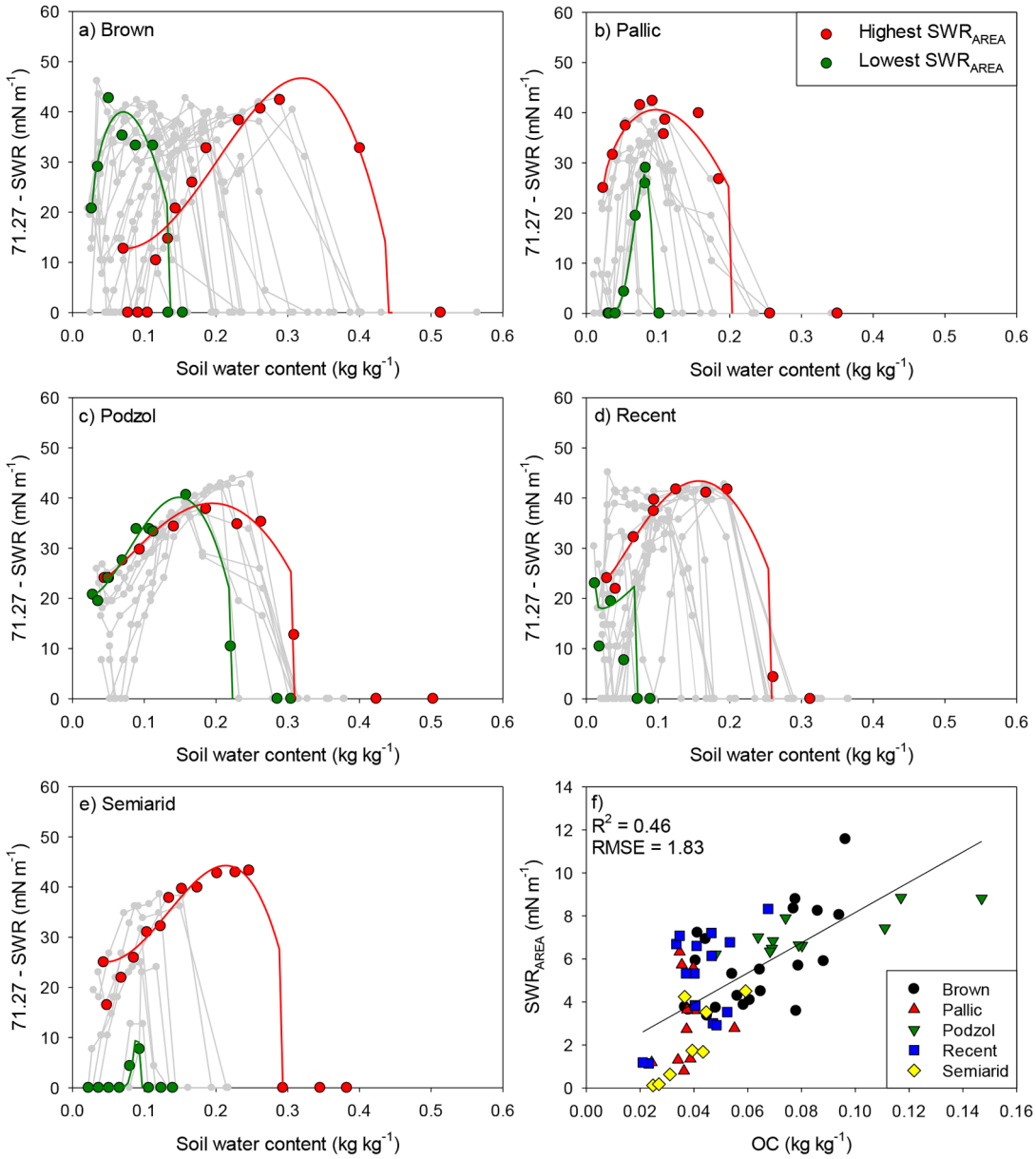

Fig. 4. (a–e) Soil water repellency (SWR) versus water content (*w*) curves for each soil order, with the minimum and maximum trapezoidal integrated area underneath the soil water repellency versus water content curve (SWR$_{AREA}$) highlighted. The fit of the Karunarathna et al. (2010a) function is illustrated for the minimum and maximum SWR$_{AREA}$. (f) The SWR$_{AREA}$ obtained from the Karunarathna et al. (2010a) function fit as a function of organic carbon (OC) content. R^2, coefficient of determination; RMSE, root mean square error.

584 and 602 nm. Knowing that organic matter absorbs light within this interval (Ben-Dor et al., 1997), this plateau might be caused by the comparably high organic matter content of the Podzols. Within the near-infrared range, all soil orders had peaks at 1415 nm and around 1922 to 1927 nm, which could be attributed to the OH stretch and HOH bend (Hunt, 1977; Knadel et al., 2014). Between these two peaks, the Podzols had a relatively small peak at 1726 nm, which has been associated with the aliphatic C–H stretch in soil organic matter. There was a common peak for all soil orders around 2208 to 2214 nm, which is associated with an Al–OH bend and OH stretch combination (Viscarra Rossel et al., 2006). Finally, there was a peak at 2352 nm, which could be related to the C–H bond in soil organic matter (Ben-Dor et al., 1997).

iPLSR Intervals

The variable selection method iPLSR was used for identifying important spectral intervals in the vis-NIRS prediction of each of the parameters: the Karunarathna et al. (2010a) function (71.27 – SWR$_{MAX}$, w'_{MAX}, and w'_{NON}), the SWR$_{AREA}$ (Approach I) and OC content. In our study, we obtained the highest prediction accuracy for each of these when using interval sizes of, respectively, 60, 45, 55, 65, and 70 nm. Since the spectral sampling interval was 0.5 nm, these interval sizes corresponded to intervals of 120, 90, 110, 130, and 140 variables. The optimal iPLSR interval size depends on both the spectral pretreatment procedure and the soil property to be predicted. A previous study, which applied Savitzky Golay first- or second-derivative spectral pretreatment and iPLSR to predict fitting parameters of a par-

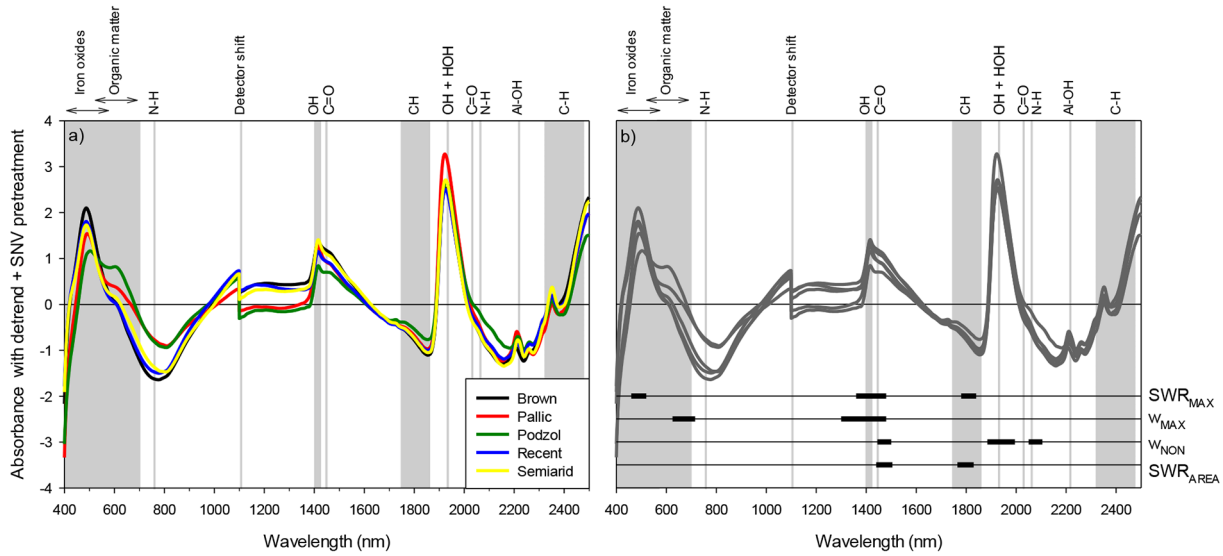

Fig. 5. (a) Visible near-infrared spectroscopy (vis-NIRS) spectra pretreated by detrending (third order) and standard normal variate (SNV). The spectra presented are averages for each soil order. (b) Spectral intervals used for the vis-NIRS cross-validation models obtained by interval partial least squares regression. Horizontal lines denote the spectral intervals used for the maximum level of SWR (SWR_{MAX}), the water content at SWR_{MAX} (w_{MAX}), the critical soil water content (w_{NON}) and the integrated area underneath the soil water repellency versus water content curve (SWR_{AREA}).

ticle-size distribution function using vis-NIRS reported optimal interval sizes between 40 and 50 nm (Hermansen et al., 2017), which is comparable to the interval sizes applied in this study.

We included three spectral intervals to predict 71.27 – SWR_{MAX} (460–520, 1360–1480, and 1780–1840 nm), two spectral intervals for w_{MAX} (625–715 and 1300–1480 nm), three spectral intervals for w_{NON} (1445–1500, 1885–1995, and 2050–2105 nm), two spectral intervals for SWR_{AREA} (Approach I) (1440–1505 and 1765–1830 nm), and two spectral intervals for OC (1380–1450 and 1590–1660 nm) (Fig. 5b). Throughout the visible range, the vis-NIRS model for 71.27 – SWR_{MAX} in the selected spectral interval might be utilizing information from the electronic transition of iron oxides within the range 460 to 520 nm (Hunt, 1977; Scheinost et al., 1998; Stenberg et al., 2010). Further, the vis-NIRS model for w_{MAX} might be utilizing information from iron oxides or organic matter in the interval 625 to 715 nm (Ben-Dor et al., 1997; Scheinost et al., 1998). This is in accordance with the study of Kim et al. (2014) who found that bands around 457, 622, and 670 nm positively influenced the vis-NIRS prediction of SWR after oven-drying at 65°C. Further, Knadel et al. (2016) found the 620 nm band to be important for predicting SWR after oven-drying at 60 and 105°C. In the near-infrared range, all models included a spectral interval that either overlapped (71.27 – SWR_{MAX}: 1360–1480 nm, w_{MAX}: 1300–1480 nm, OC: 1380–1450 nm) or appeared just after (w_{NON}: 1445–1500 nm, SWR_{AREA}: 1440–1505 nm) the characteristic absorption band for OH stretching around 1400 nm (Hunt, 1977). Thus, based on the overlapping intervals, the spectral region around 1300 to 1500 nm appears to be important for SWR prediction (Fig. 5b). This spectral region contains absorption features from OH in clay minerals (e.g., around 1415 nm) (Viscarra Rossel et al., 2006), OH in organic components such as cellulose, lignin or starch around 1358 nm (Ben-Dor et al., 1997) and carboxylic acids around 1449 nm (Viscarra Rossel et al., 2006). Although OC is considered as the main soil property controlling the severity of SWR (Hermansen et al., 2019), it has been shown that the correlation between SWR_{AREA} and OC can be slightly improved when omitting the amount of OC complexed by clay (de Jonge et al., 2009). In that sense, the vis-NIRS spectral information about clay minerals might be relevant to predict SWR. Previous studies also suggested that spectral information of clay minerals assist SWR prediction with vis-NIRS (Kim et al., 2014; Knadel et al., 2016). Knadel et al. (2016) identified a wide band from 1000–1490 nm in a regression coefficient SWR determination, which further supports the view that this wide absorption region carries important SWR information. The iPLSR intervals for 71.27 – SWR_{MAX} and SWR_{AREA} furthermore had some overlap (71.27 – SWR_{MAX}: 1780–1840 nm, SWR_{AREA}: 1765–1830 nm), indicating that this spectral region also carries important information for SWR prediction, characterized especially by absorptions from the C–H stretch in organic matter (Viscarra Rossel and Behrens, 2010). When comparing to Kim et al. (2014) study, Knadel et al. (2016) also found the band around 1765 nm to positively assist in SWR prediction. The iPLSR interval for w_{NON} from 1885 to 1995 nm overlaps the characteristic absorption band from the OH stretch and HOH bend (Hunt, 1977). This interval also contains information from carboxylic acids (Ben-Dor et al., 1997). Finally, for w_{NON} the iPLSR interval from 2050 to 2105 nm is located in the spectral range that includes absorptions from amines or amides (Viscarra Rossel and Behrens, 2010).

Vis-NIRS Predictions of Soil Water Repellency vs. Water Content Curves

In this study, cross-validation was used as validation method, although cross-validation might overestimate the accuracy of the model as compared to an independent validation. However, cross-validation was considered to be a sufficient validation method to investigate the predictive ability for the SWR-*w*

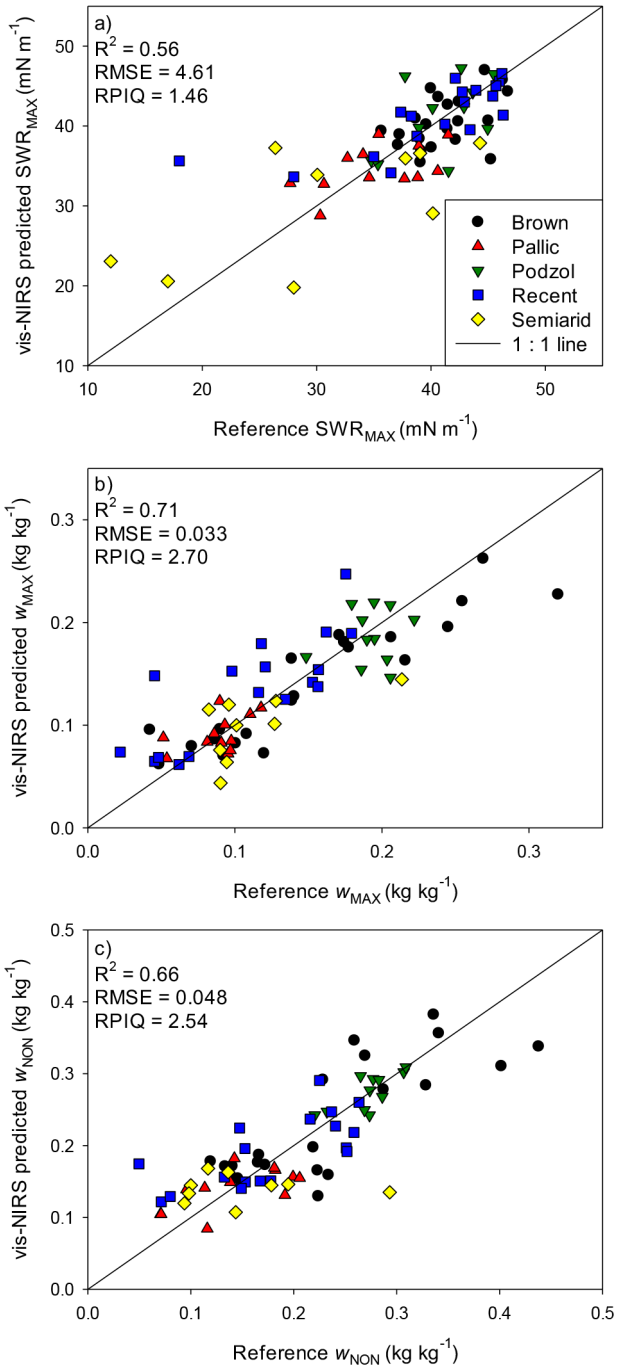

Fig. 6. Visible near-infrared spectroscopy (vis-NIRS) cross-validation models (n = 71) for the three fitting parameters of the Karunarathna et al. (2010a) model: (a) maximum level of SWR (SWR_{MAX}), (b) water content at SWR_{MAX} (w_{MAX}), and (c) critical soil water content (w_{NON}). R^2, coefficient of determination; RMSE, root mean square error; RPIQ, ratio of performance to interquartile range.

curve, since the dataset covered many soil types and a wide spatial distribution across New Zealand's South Island.

We tested the ability of the vis-NIRS spectra to predict OC content to see whether we could expect a reasonable result for SWR parameters, which are related to OC content. The OC content was successfully predicted with an R^2 of 0.75 and RMSECV of 0.012 kg kg^{-1} using 11 factors. Further, we could predict the fitting parameters of Eq. [1] using vis-NIRS (Fig. 6). The cross-validation model for 71.27 – SWR_{MAX} gave values for R^2 of 0.56 and RMSECV of 4.61 mN m^{-1}, for w_{MAX} corresponding values were, respectively, 0.71 and 0.033 kg kg^{-1}, and for the w_{NON} model they were 0.66 and 0.048 kg kg^{-1} (Table 2). The vis-NIRS prediction of SWR_{MAX} exhibited increasing scatter around the 1:1 line with decreasing SWR_{MAX}, which might be caused by the low density of soils within the low SWR_{MAX} range. Based on RPIQ values, SWR_{MAX} was predicted with the lowest accuracy (RPIQ = 1.46, Fig. 6a), whereas the accuracies for w_{MAX} (RPIQ = 2.70, Fig. 6b) and w_{NON} (RPIQ = 2.54, Fig. 6c) were comparable.

Table 2. Visible near-infrared spectroscopy (vis-NIRS) models for the three fitting parameters for the Karunarathna et al. (2010a) model: maximum level of SWR (71.27 – SWR_{MAX}), water content at 71.27 – SWR_{MAX} (w_{MAX}), critical soil water content (w_{NON}). The statistics of the vis-NIRS model for the trapezoidal integrated area underneath the soil water repellency versus water content curve (SWR_{AREA}) is given for Approach I.

Statistic	71.27 – SWR_{MAX}	w_{MAX}	w_{NON}	SWR_{AREA}
	mN m^{-1}	kg kg^{-1}	kg kg^{-1}	mN m^{-1} kg kg^{-1}
		Calibration		
Mean	38.42	0.133	0.201	4.95
RMSEC †	3.72	0.028	0.041	1.44
R^2 ‡	0.71	0.79	0.75	0.66
Factors	11	10	8	5
		Cross-validation		
RMSECV §	4.61	0.033	0.048	1.62
R^2	0.56	0.71	0.66	0.58
RPIQ ¶	1.46	2.70	2.54	1.98

† RMSEC, root mean square error of calibration.
‡ R^2, coefficient of determination.
§ RMSECV, root mean square error of cross-validation.
¶ RPIQ, ratio of performance to interquartile range.

The vis-NIRS-predicted values for 71.27 – SWR_{MAX}, w_{MAX}, and w_{NON} and the measured SWR_{AD} and w_{AD} were used as input parameters to Eq. [1] to yield vis-NIRS-predicted SWR-w curves (Fig. 7). As can be seen from Fig. 6b and 6c, there was some scatter around the 1:1 line, which caused some of the predictions for w_{MAX} and w_{NON} to overlap for the four unsuccessfully predicted SWR-w curves. Especially the shape of the SWR-w curves for soils within the Brown, Recent and Podzol soil orders were successfully predicted with few exceptions (e.g., Fig. 7a, 7l, and 7x). The SWR-w curves for the soils within the Semiarid soil order were not as accurately vis-NIRS-predicted. The Semiarid soils caused some scattering in the SWR_{MAX} prediction, and therefore the less accurate prediction of this fitting parameter also affected the overall shape of the vis-NIRS-predicted SWR-w curves. But in general, we succeeded in predicting the extent and shape of SWR-w curves across a dataset with a wide distribution in texture and OC.

The SWR_{AREA} was vis-NIRS-predicted using two approaches. The accuracy for the SWR_{AREA} Approach II can be seen as verification of how well the vis-NIRS-predicted SWR-w curves fitted onto the reference Karunarathna et al. (2010a) function (Fig. 8b). Approach I resulted in an R^2 of 0.58 and RMSECV of 1.62 mN m^{-1} kg kg^{-1}, and Approach II resulted in an R^2 of 0.56 and RMSECV of 1.70 mN m^{-1} kg kg^{-1} (Fig. 8). Since the vis-NIRS-prediction for SWR_{AREA} in Approach I ob-

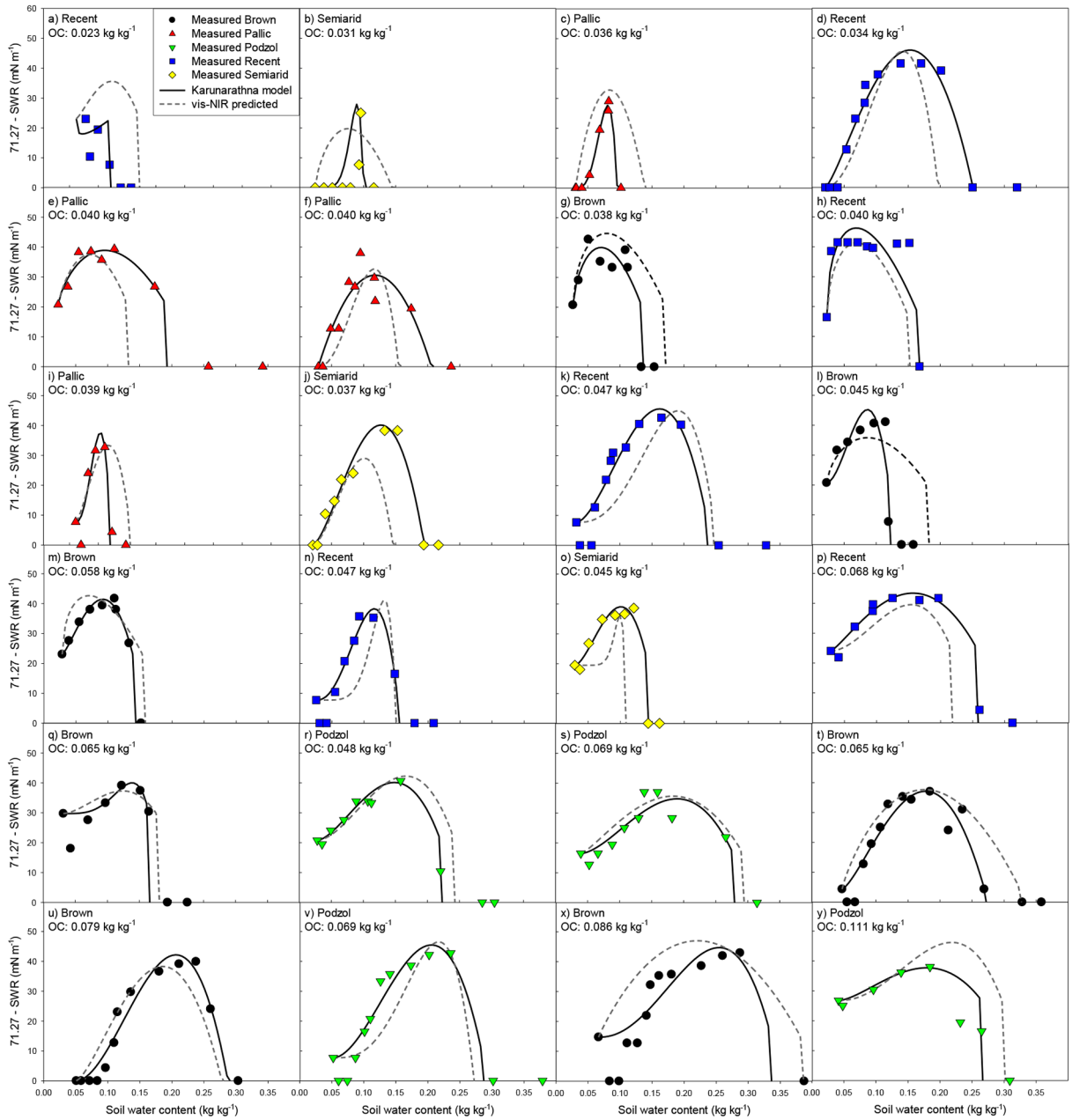

Fig. 7. Soil water repellency (SWR) versus water content curves. Each box represents one of three replicates from the 24 locations (two locations were excluded because they were hydrophilic). For each soil sample, the discrete SWR measurements are shown together with the continuous curve fit using the Karunarathna et al. (2010a) model and the curve obtained by predicting the three Karunarathna et al. (2010a) model fitting parameters with visible near-infrared spectroscopy (vis-NIRS).

tained a slightly higher accuracy and simultaneously was based on less parameters, Approach I is recommended to obtain the SWR_{AREA} from vis-NIRS. Compared to the correlation between SWR_{AREA} and OC (Fig. 4f), vis-NIRS performed better than OC in describing the variation in SWR_{AREA} for this dataset. The higher accuracy of vis-NIRS for the SWR_{AREA} might be caused by the additional information about OC quality embedded in the vis-NIRS spectra compared to the SWR_{AREA} vs. OC regression which only takes into account the total amount of OC.

One of the main reasons for the successful application of vis-NIRS to predict SWR parameters is the correlation between SWR_{AREA} and OC content with the latter being spectrally active. All soil samples in this study were collected from areas under pasture. Earlier studies, found that perennial grass can result in higher severities in SWR as compared to the severity found in similar soils under barley and wheat (de Jonge et al., 2007; de Jonge et al., 2009). Future studies should investigate whether the vis-NIR models are applicable across geographical regions and land uses.

CONCLUSION

In this study, we predicted SWR-*w* curves for soil samples covering a wide range in OC and texture, by combining vis-NIR spectroscopy and the Karunarathna et al. (2010a) empirical β function, which was fitted to the SWR-*w* curve between w_{AD} and w_{NON}.

With acceptable accuracy, we could predict the three fitting parameters of the Karunarathna et al. (2010a) function (R^2

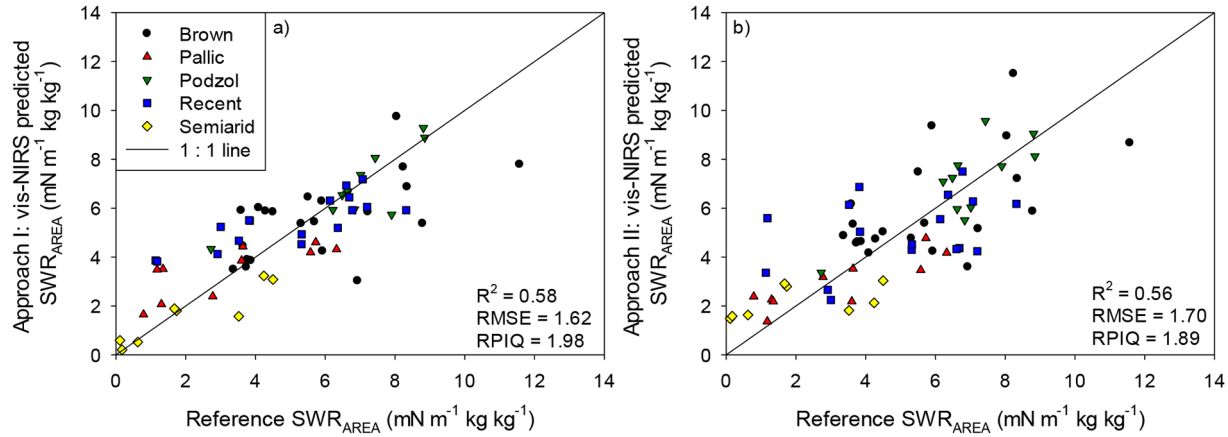

Fig. 8. Visible near-infrared spectroscopy (vis-NIRS) predictions of the trapezoidal integrated area underneath the soil water repellency (SWR) versus water content (*w*) curve (SWR_{AREA}) using two different approaches on 67 samples. (a) A vis-NIRS cross-validation model was developed on SWR_{AREA} values obtained from the Karunarathna et al. (2010a) model fit (Approach I). (b) A total of three vis-NIRS cross-validation models were developed for each of the three Karunarathna et al. (2010a) model fitting parameters (SWR_{MAX}, w_{MAX}, and w_{NON}), which were used to obtain vis-NIRS-predicted SWR-*w* curves, from which the SWR_{AREA} could be obatined (Approach II). R^2, coefficient of determination; RMSE, root mean square error; RPIQ, ratio of performance to interquartile range.

from 0.56 to 0.71), namely the highest severity in SWR a soil can exhibit (71.27 − SWR_{MAX}), the *w* at which the soil is most water repellent (w_{MAX}), and the *w* above which the soil becomes hydrophilic (w_{NON}).

The vis-NIRS predictions of 71.27 − SWR_{MAX}, w_{MAX}, and w_{NON} served then as input values to the Karunarathna et al. (2010a) function together with measured values of air-dry water content (w_{AD}) and the severity in SWR at air-dried conditions (SWR_{AD}) to yield vis-NIRS-predicted SWR-*w* curves. The curves obtained from vis-NIRS represented the reference fit of the Karunarathna et al. (2010a) function well. The SWR_{AREA} obtained from the Karunarathna et al. (2010a) reference fit could further be vis-NIRS-predicted with an R^2 of 0.58 and RMSECV of 1.62 mN m^{-1} kg kg^{-1}.

In conclusion, one vis-NIRS scan and one SWR measurement at air-dried conditions is sufficient to predict the shape of the SWR-*w* curve and SWR_{AREA} for these soils. Further studies will test whether a similar approach can be applied to obtain SWR-w curves from vis-NIRS on soil samples from different geographic regions and land uses.

ACKNOWLEDGMENTS

This project was funded by the Aarhus University Research Foundation grant (AUFF-E-2016-9-36). Further, the project was funded by the European Union's Horizon 2020 Research and Innovation Project 'PROTINUS' (Grant No. 645717) with counter-funding from the Royal Society of New Zealand.

REFERENCES

Andersen, C.M., and R. Bro. 2010. Variable selection in regression—a tutorial. J. Chem. 24:728–737. doi:10.1002/cem.1360

Babaeian, E., M. Homaee, H. Vereecken, C. Montzka, A.A. Norouzi, and M.T. van Genuchten. 2015. A comparative study of multiple approaches for predicting the soil-water retention curve: Hyperspectral information vs. basic soil properties. Soil Sci. Soc. Am. J. 79:1043–1058. doi:10.2136/sssaj2014.09.0355

Bachmann, J., M. Deurer, and G. Arye. 2007. Modeling water movement in heterogeneous water-repellent soil: 1. Development of a contact angle-dependent water-retention model. Vadose Zone J. 6:436–445. doi:10.2136/vzj2006.0060

Barnes, R.J., M.S. Dhanoa, and S.J. Lister. 1989. Standard normal variate transformation and de-trending of near-infrared diffuse reflectance spectra. J. Appl. Spectrosc. 43:772–777. doi:10.1366/0003702894202201

Bellon-Maurel, V., E. Fernandez-Ahumada, B. Palagos, J.M. Roger, and A. McBratney. 2010. Critical review of chemometric indicators commonly used for assessing the quality of the prediction of soil attributes by NIR spectroscopy. TrAC. Trends Analyt. Chem. 29:1073–1081. doi:10.1016/j.trac.2010.05.006

Ben-Dor, E., Y. Inbar, and Y. Chen. 1997. The reflectance spectra of organic matter in the visible near-infrared and short wave infrared region (400–2500 nm) during a controlled decomposition process. Remote Sens. Environ. 61:1–15. doi:10.1016/S0034-4257(96)00120-4

Blakemore, L., P.L. Searle, and B.K. Dalby. 1987. Methods for chemical analysis of soils. New Zealand Soil Bureau Scientific Report No. 80, New Zealand Soil Bureau, Wellington.

Chang, C.W., D.A. Laird, M.J. Mausbach, and C.R. Hurburgh. 2001. Near-infrared reflectance spectroscopy–principal components regression analyses of soil properties. Soil Sci. Soc. Am. J. 65:480–490. doi:10.2136/sssaj2001.652480x

Clark, R.N. 1999. Spectroscopy of rocks and minerals and principles of spectroscopy. In: A.N. Rencz, editor, Remote sensing for the earth sciences: Manual of remote sensing. John Wiley & Sons, Chichester, UK. p. 3–58.

de Jong, S. 1993. SIMPLS: An alternative approach to partial least squares regression. Chemom. Intell. Lab. Syst. 18:251–263. doi:10.1016/0169-7439(93)85002-X

de Jonge, L.W., O.H. Jacobsen, and P. Moldrup. 1999. Soil water repellency: Effects of water content, temperature, and particle size. Soil Sci. Soc. Am. J. 63:437–442. doi:10.2136/sssaj1999.03615995006300030003x

de Jonge, L.W., P. Moldrup, and O.H. Jacobsen. 2007. Soil-water content dependency of water repellency in soils: Effect of crop type, soil management, and physical-chemical parameters. Soil Sci. 172:577–588. doi:10.1097/SS.0b013e318065c090

de Jonge, L.W., P. Moldrup, and P. Schjonning. 2009. Soil infrastructure, interfaces & translocation processes in inner space ('soil-it-is'): Towards a road map for the constraints and crossroads of soil architecture and biophysical processes. Hydrol. Earth Syst. Sci. 13:1485–1502. doi:10.5194/hess-13-1485-2009

Dekker, L.W., and C.J. Ritsema. 1995. Fingerlike wetting patterns in two water-repellent loam soils. J. Environ. Qual. 24:324–333. doi:10.2134/jeq1995.00472425002400020016x

Deurer, M., K. Müller, C. Van den Dijssel, K. Mason, J. Carter, and B.E. Clothier. 2011. Is soil water repellency a function of soil order and proneness to drought? A survey of soils under pasture in the North Island of New Zealand. Eur. J. Soil Sci. 62:765–779. doi:10.1111/j.1365-2389.2011.01392.x

Doerr, S.H., R.A. Shakesby, and R.P.D. Walsh. 2000. Soil water repellency: Its

causes, characteristics and hydro-geomorphological significance. Earth Sci. Rev. 51:33–65. doi:10.1016/S0012-8252(00)00011-8

Franco, C.M.M., M.E. Tate, and J.M. Oades. 1995. Studies on non-wetting sands. I. The role of intrinsic particulate organic matter in the development of water-repellency in non-wetting sands. Aust. J. Soil Res. 33:253–263. doi:10.1071/SR9950253

Graber, E.R., S. Tagger, and R. Wallach. 2009. Role of divalent fatty acid salts in soil water repellency. Soil Sci. Soc. Am. J. 73:541–549. doi:10.2136/sssaj2008.0131

Hermansen, C., M. Knadel, P. Moldrup, M.H. Greve, R. Gislum, and L.W. de Jonge. 2016. Visible–near-infrared spectroscopy can predict the clay/organic carbon and mineral fines/organic carbon ratios. Soil Sci. Soc. Am. J. 80:1486–1495. doi:10.2136/sssaj2016.05.0159

Hermansen, C., M. Knadel, P. Moldrup, M.H. Greve, D. Karup, and L.W. de Jonge. 2017. Complete soil texture is accurately predicted by visible near-infrared spectroscopy. Soil Sci. Soc. Am. J. 81:758–769. doi:10.2136/sssaj2017.02.0066

Hermansen, C., P. Moldrup, K. Müller, P.W. Jensen, C. Van den Dijssel, P. Jeyakumar, and L.W. de Jonge. 2019. Organic carbon content controls the severity of water repellency and the critical moisture level across New Zealand pasture soils. Geoderma 338:281–290. doi:10.1016/j.geoderma.2018.12.007

Hewitt, A. 2013. Survey of New Zealand soil orders. In: J.R. Dymond, editor, Ecosystem services in New Zealand: Conditions and trends. Manaaki Whenua Press, Lincoln, New Zealand. p. 121–131.

Hewitt, A.E. 2010. New Zealand soil classification. Landcare Research Science Series No. 1. 3rd ed. Manaaki Whenua Press, Lincoln, New Zealand.

Hunt, G.R. 1977. Spectral signatures of particulate minerals in the visible and near infrared. Geophysics 42:501–513. doi:10.1190/1.1440721

IUSS Working Group WRB. 2006. World Reference Base for Soil Resources 2006. A framework for international classification, correlation and communication, Second ed. FAO, Rome.

Karunarathna, A.K., K. Kawamoto, P. Moldrup, L.W. de Jonge, and T. Komatsu. 2010a. A simple beta-function model for soil-water repellency as a function of water and organic carbon contents. Soil Sci. 175:461–468. doi:10.1097/SS.0b013e3181f55ab6

Karunarathna, A.K., P. Moldrup, K. Kawamoto, L.W. de Jonge, and T. Komatsu. 2010b. Two-region model for soil water repellency as a function of matric potential and water content. Vadose Zone J. 9:719–730. doi:10.2136/vzj2009.0124

Katuwal, S., C. Hermansen, M. Knadel, P. Moldrup, M.H. Greve, and L.W. de Jonge. 2018. Combining x-ray computed tomography and visible near-infrared spectroscopy for prediction of soil structural properties. Vadose Zone J. 17. doi:10.2136/vzj2016.06.0054

Kawamoto, K., P. Moldrup, T. Komatsu, L.W. de Jonge, and M. Oda. 2007. Water repellency of aggregate size fractions of a volcanic ash soil. Soil Sci. Soc. Am. J. 71:1658–1666. doi:10.2136/sssaj2006.0284

Kim, I., R.R. Pullanagari, M. Deurer, R. Singh, K.Y. Huh, and B.E. Clothier. 2014. The use of visible and near-infrared spectroscopy for the analysis of soil water repellency. Eur. J. Soil Sci. 65:360–368. doi:10.1111/ejss.12138

King, P.M. 1981. Comparison of methods for measuring severity of water repellence of sandy soils and assessment of some factors that affect its measurement. Aust. J. Soil Res. 19:275–285. doi:10.1071/SR9810275

Knadel, M., F. Deng, A. Thomsen, and M.H. Greve. 2012. Development of a Danish national vis-NIR soil spectral library for soil organic carbon determination. Digital Soil Assess. Beyond:403-408. doi:10.1201/b12728-79

Knadel, M., F. Deng, A. Alinejadian, L.W. de Jonge, P. Moldrup, and M.H. Greve. 2014. The effects of moisture conditions - from wet to hyper dry - on visible near-infrared spectra of Danish reference soils. Soil Sci. Soc. Am. J. 78:422–433. doi:10.2136/sssaj2012.0401

Knadel, M., F. Masis-Meléndez, L.W. de Jonge, P. Moldrup, E. Arthur, and M.H. Greve. 2016. Assessing soil water repellency of a sandy field with visible near infrared spectroscopy. J. Near Infrared Spectrosc. 24:215–224. doi:10.1255/jnirs.1188

Knadel, M., E. Arthur, P. Weber, P. Moldrup, M.H. Greve, Z.P. Chrysodonta, and L.W. de Jonge. 2018. Soil specific surface area determination by visible near-infrared spectroscopy. Soil Sci. Soc. Am. J. 82:1046–1056. doi:10.2136/sssaj2018.03.0093

Leighton-Boyce, G., S.H. Doerr, R.A. Shakesby, and R.P.D. Walsh. 2007. Quantifying the impact of soil water repellency on overland flow generation and erosion: A new approach using rainfall simulation and wetting agent on in situ soil. Hydrol. Processes 21:2337–2345. doi:10.1002/hyp.6744

Müller, K., M. Deurer, M. Slay, T. Aslam, J.A. Carter, and B.E. Clothier. 2010. Environmental and economic consequences of soil water repellency under pasture. Proc. N. Z. Grassl. Assoc. 72:207-210.

Müller, K., M. Deurer, K. Kawamoto, T. Kuroda, S. Subedi, S. Hiradate, T. Komatsu, and B.E. Clothier. 2014. A new method to quantify how water repellency compromises soils' filtering function. Eur. J. Soil Sci. 65:348–359. doi:10.1111/ejss.12136

Nørgaard, L., A. Saudland, J. Wagner, J.P. Nielsen, L. Munck, and S.B. Engelsen. 2000. Interval partial least-squares regression (iPLS): A comparative chemometric study with an example from near-infrared spectroscopy. Appl. Spectrosc. 54:413–419. doi:10.1366/0003702001949500

Osborn, J.F., R.E. Pelishek, J.S. Krammes, and J. Letley. 1964. Soil wettability as a factor in erodibility. Soil Sci. Soc. Am. J. 28:294–295. doi:10.2136/sssaj1964.03615995002800020050x

Peng, Y., M. Knadel, R. Gislum, K. Schelde, A. Thomsen, and M.H. Greve. 2014. Quantification of SOC and clay content using visible near-infrared reflectance–mid-infrared reflectance spectroscopy with Jack-Knifing partial least squares regression. Soil Sci. 179:325–332. 10.1097/Ss.0000000000000074

Pittaki-Chrysodonta, Z., P. Moldrup, M. Knadel, B.V. Iversen, C. Hermansen, M.H. Greve, and L.W. de Jonge. 2018. Predicting the Campbell soil water retention function: Comparing visible–near-infrared spectroscopy with classical pedotransfer function. Vadose Zone J. 17. doi:10.2136/vzj2017.09.0169

Regalado, C.M., and A. Ritter. 2005. Characterizing water dependent soil repellency with minimal parameter requirement. Soil Sci. Soc. Am. J. 69:1955–1966. doi:10.2136/sssaj2005.0060

Regalado, C.M., and A. Ritter. 2009a. A soil water repellency empirical model. Vadose Zone J. 8:136–141. doi:10.2136/vzj2008.0097

Regalado, C.M., and A. Ritter. 2009b. A bimodal four-parameter lognormal linear model of soil water repellency persistence. Hydrol. Processes 23:881–892. doi:10.1002/hyp.7226

Regalado, C.M., A. Ritter, L.W. de Jonge, K. Kawamoto, T. Komatsu, and P. Moldrup. 2008. Useful soil-water repellency indices: Linear correlations. Soil Sci. 173:747–757. doi:10.1097/SS.0b013e31818d4163

Roy, J.L., and W.B. McGill. 2000. Flexible conformation in organic matter coatings: An hypothesis about soil water repellency. Can. J. Soil Sci. 80:143–152. doi:10.4141/S98-093

Roy, J.L., and W.B. McGill. 2002. Assessing soil water repellency using the molarity of ethanol droplet (MED) test. Soil Sci. 167:83–97. doi:10.1097/00010694-200202000-00001

Savitzky, A., and M.J.E. Golay. 1964. Smoothing and differentiation of data by simplified least squares procedures. Anal. Chem. 36:1627–1639. doi:10.1021/ac60214a047

Scheinost, A.C., A. Chavernas, V. Barron, and J. Torrent. 1998. Use and limitations of second-derivative diffuse reflectance spectroscopy in the visible to near-infrared range to identify and quantify Fe oxide minerals in soils. Clays Clay Miner. 46:528–536. doi:10.1346/CCMN.1998.0460506

Stenberg, B., R.A. Viscarra Rossel, A.M. Mouazen, and J. Wetterlind. 2010. Visible and near infrared spectroscopy in soil science. Adv. Agron. 107:163–215. doi:10.1016/S0065-2113(10)07005-7

Viscarra Rossel, R.A., and T. Behrens. 2010. Using data mining to model and interpret soil diffuse reflectance spectra. Geoderma 158:46–54. doi:10.1016/j.geoderma.2009.12.025

Viscarra Rossel, R.A., R.N. McGlynn, and A.B. McBratney. 2006. Determining the composition of mineral-organic mixes using UV-vis-NIR diffuse reflectance spectroscopy. Geoderma 137:70–82. doi:10.1016/j.geoderma.2006.07.004

Zou, X., J. Zhao, M.J.W. Povey, M. Holmes, and H. Mao. 2010. Variables selection methods in near-infrared spectroscopy. Anal. Chim. Acta 667:14–32. doi:10.1016/j.aca.2010.03.048